# PS-b-PMMA Block Copolymer Derived Electrospun Nanofibers: Synthesis, Characterization and Surface Properties Evaluation

## Akanksha Adaval

A Dissertation Submitted to

Indian Institute of Technology Hyderabad

In Partial Fulfillment of the Requirements for

The Degree of Master of Technology



भारतीय प्रौद्योगिकी संस्थान हैदराबाद
**Indian Institute of Technology Hyderabad**

Department of Chemical Engineering

June, 2014

## Declaration

I declare that this written submission represents my ideas in my own words, and where others' ideas or words have been included, I have adequately cited and referenced the original sources. I also declare that I have adhered to all principles of academic honesty and integrity and have not misrepresented or fabricated or falsified any idea/data/fact/source in my submission. I understand that any violation of the above will be a cause for disciplinary action by the Institute and can also evoke penal action from the sources that have thus not been properly cited, or from whom proper permission has not been taken when needed.

(Signature)

Akanksha
CH12M1001

# Approval Sheet

This thesis entitled "**PS-b-PMMA Block Copolymer Derived Electrospun Nanofibers: Synthesis, Characterization and Surface Properties Evaluation**" by Akanksha Adaval is approved for the degree of Master of Technology from IIT Hyderabad.

Dr Subha Narayan Rath

Department of Biomedical Enginnering

Indian Institute of Technology Hyderabad

Examiner

Dr Saptarshi Majumdar

Department of Chemical Engineering

Indian Institute of Technology Hyderabad

Examiner

Dr Debaprasad Shee

Department of Chemical Engineering

Indian Institute of Technology Hyderabad

Examiner

Dr Chandra Shekhar Sharma

Department of Chemical Engineering

Indian Institute of Technology Hyderabad

Advisor

iii

# Acknowledgements

Dedicated to

My Family and Friends

# Abstract

Block copolymers represent a broad subject of current research due to their exotic property of controlled micro phase separation which paves way to fabricate periodic nanostructures that can be utilized in various engineering applications. Electrospinning of block copolymers to produce nanofibers is an emerging area which is simple and efficient for nanofiber production. The nanofibers with their high surface area and increased mechanical properties can be combined with the unique properties of block copolymers for use in numerous applications like filtration, biosensors, drug delivery, tissue engineering and protective clothing. In this work poly(styrene-block-methylmethacrylate) (PS-b-PMMA) was electrospun in an organic solvent and optimized a number of electrospinning parameters that affect the morphology of the obtained non-woven fabric such as concentration, applied electric field, distance between the source and collector and flow rate in order to yield long, continuous and uniform nanofibers. Thereafter, as-spun fibers were annealed by two methods such as thermal and using solvent assisted vapors. UV exposure to the annealed fibers were done to allow the phase separation of polymer blocks and complete the cross-linking of one phase. The non crosslinked phase was subsequently etched out selectively using a weak acid in order to generate the porosity in the PS-b-PMMA electrospun fiber mats. FESEM, FTIR spectroscopy and TGA were used for structural characterization of electrospun PS-b-PMMA fibers and the effect on the morphology of obtained fibers was observed by changing the different electrospinning parameters. We further studied the wettability characteristics using contact angle goniometer which showed that changing morphology affects the wettability. A comparative study on the reflectivity properties of as spun, beaded fibers and etched fibers revealed that the anti-reflectivity characteristics shown by as-spun fibers were the highest. Further, adsorption studies of a dye methylene blue were carried out with ACF fabric and fibers deposited on ACF fabric. Effect of changing the concentration of adsorbate, changing time and temperature was studied. The fibers showed higher adsorption capability compared to ACF fabric showing improved adsorption efficiency.

# Nomenclature

| | |
|---|---|
| nm | Nanometer |
| PS-b-PMMA | Polystyrene-b-poly(methylmethacrylate) |
| PEG-b-PS | Polyethylene glycol-b-polystryrene |
| PS-b-PPG | Polystyrene-b-polypropylene glycol |
| DMF | Dimethylformamide |
| (PF-b-PNIPAAm-b-PNMA) | (Polyfluorene-b-poly(N-isopropylacrylamide)-b-poly(N-methylolacrylamide)) |
| PLGA | Poly(lactide-co-glycolide) |
| PLA-b-PEG-b-PLA | Polylactic acid-b-polyethylene glycol-b-polylactic acid |
| PEG-b-PCL | Polyethylene-b-polycaprolactone |
| SEM | Scanning Electron Microscope |
| PS-b-PNIPAM-b-PS | Polystyrene-b-poly(N-methylolacrylamide)-b-polystyrene |
| BCP | Block copolymer |
| THF | Tetrahydrofuran |
| $M_w$ | Weight molecular average |
| $M_n$ | Number molecular average |
| UV | Ultraviolet |
| FTIR | Fourier Transform Infrared Radiation |
| TGA | Thermogravimetric analysis |
| SDFCL | S D Fine-Chem Limited |
| ml | milliliter |
| kV | kilovolts |
| μl | microliter |
| cm | centimeter |
| DI | De-ionized (water) |
| mm | millimeter |
| ATR | Attenuated Total Reflection |

| | |
|---|---|
| $\chi_{AB}$ | Interaction parameter |
| $\Upsilon_{SG}$ | Interfacial tension between solid and liquid medium |
| $\Upsilon_{LG}$ | Interfacial tension between liquid and vapor medium |
| $\Upsilon_{SL}$ | Interfacial tension between solid and vapor medium |
| $\cos\theta$ | Contact angle |
| ppm | Parts per million |
| ACF | Activated Carbon Fabric |
| mg/l | Milligram per litre |

# Contents

# Chapter 1
# Introduction

## 1.1 Electrospun Nanofibers

Nanofibers are defined as fibers with diameters less than 100 nanometers. Unlike other 1D nanostructures, such as nanotubes and nanowires, nanofibers exhibit a wide range of unique properties such as high surface-to-volume ratio, high mechanical strength and surface functionalities. Nanofibers having low density, large surface area to mass, high pore volume, and tight pore size make them appropriate to be used in many applications such as filtration, catalysis, sensing, protective clothing, tissue engineering scaffolds and nano-electronics [1, 2]. Thus, nanofibers with their high surface area to volume ratio, have the potential to significantly improve current technology and find application in new areas. A multitude of strategies like electrospinning [3], template synthesis and self-assembly [4-6] are the most frequently used methods to produce nanofibers.

In recent years electrospinning has emerged as a technique to make ultrafine continuous fibers which range from 10 − 1000 nm. The term electrospinning has been derived from the word electrostatic spinning which means using electrostatic force for the production of polymer filaments. Around 1944 Formhals described an experimental setup for the same. It is a relatively easy, efficient and robust method which uses a variety of materials to produce 1D nanostructures. It provides the unique ability to produce nanofibers of different materials in various fiber

assemblies. It has a relatively simple setup (Fig 2.1) and high production rate. This process depends on the complex interplay of many molecular parameters like solubility, molecular weight and various process parameters such as electrical conductivity, feed rate and temperature and involves the continuous stretching of polymer solution or melt when a strong electric field is applied [1]. Electrospun nanofibrous scaffolds possess high surface-to-volume ratio, tunable porosity, low cost, flexible morphology tuning and high-throughput continuous production which has made it to emerge as a technique to produce various functional fibers. Thus, a number of applications can be proposed in various areas ranging from membranes and sensors to nanocomposites, nanodevices and tissue engineering [7, 8].

## 1.1.1 Factors affecting the morphology of electrospun nanofibers

To have a clear understanding about the nature of electrospinning and the conversion of polymer solutions into nanofibers the working parameters need to be looked into. By proper controlling of these parameters, fibers with desired morphologies and diameter can be fabricated. These working parameters can be classified into three parts such as solution parameters, process parameters and ambient parameters [9].

<u>Solution Parameters</u>

1. <u>Concentration:</u> For low concentration, electrospraying occurs and there is beads formation due to low viscosity of the solution. As the concentration is increased the fiber diameter increases.

2. Molecular weight: Molecular weight signifies the entanglement of the polymer chains in the solution i.e. the solution viscosity. For low molecular weight there is beads formation and when increasing the molecular weight, smooth fibers are obtained.

3. Viscosity: Solution viscosity is an important factor for determining the fiber morphology. Continuous and smooth fibers cannot be obtained when the solution has low viscosity. For high viscosities there is hard ejection of the jets from the solution.

4. Surface Tension: It converts the liquid jet into spherical droplets to minimize the surface energy. The higher surface tension of solution at lower levels of polymer concentration causes fiber jet to fragment into droplets giving rise to beads.

5. Conductivity/Surface Charge Density:  It is mainly determined by the polymer type and the type of solvent used. Natural polymers are polyelectrolytic in nature, in which the ions increase the charge carrying ability of the polymer jet which has higher tension under the electric field resulting in the formation of poor fibers. With the aid of ionic salts small diameter fibers can be formed.

Processing Parameters

1. Voltage: Some groups reported that higher voltages facilitate the formation of large diameter fiber while some concluded that higher voltages favor the narrowing of fiber diameter. Thus, the level of the effect of voltage varies with the polymer solution concentration.

2. <u>Flow Rate</u>: For high flow rates, beaded fibers with thick diameter are formed rather than smooth fibers with thin diameter. This happens as for high flow rates the drying time is short and thus lower stretching forces which gives rise to thick fibers.

3. <u>Distance between the collector and the syringe tip</u>: Electrode separation affects the flight time and the electric field strength. If the distance is too low then beads formation takes place. While maintaining more distance the average fiber diameter decreases.

4. <u>Collectors</u>: During electrospinning, collectors act as the conductive substrate to collect the charged fibers. Al foil is usually used as a collector. Various other collectors can be used such as wire mesh, grids, parallel bar, rotating rods etc.

<u>Ambient Parameters</u>

1. <u>Humidity</u>: Low humidity dries the solvent totally and increases the solvent evaporation thus assisting in the formation of thin fibers. High humidity, on the contrary, leads to thick fiber formation owing to small stretching forces.

2. <u>Temperature:</u> On increasing the temperature the formation of thin fibers is favored as there is an inverse relation between temperature and solution viscosity.

## 1.2 Block Co-polymers

A block copolymer consists of multiple sequences or blocks of the same monomer which alternate in series with different monomer blocks. The blocks are covalently

bound to each other. Based on the number of blocks contained and their arrangement, block copolymers can be classified into different types. For example, block copolymers with two blocks are called diblocks; those with three blocks are triblocks; and those with more than three blocks are called multiblocks. For example, PS-b-PMMA is short for polystyrene-b-poly(methyl methacrylate) and is usually made by first polymerizing styrene, and then subsequently polymerizing MMA (Methyl metthacrylate) from the reactive end of the polystyrene chains. The composition of the copolymer is expressed in terms of volume fractions of the blocks. $\chi_{AB}$ is known as the interaction parameter which signifies the thermodynamic interaction between two dissimilar monomers.

The most important and unique feature of block copolymer is that it undergoes phase separation to give rise to multiple morphologies. Since the blocks in a block copolymer are covalently bonded to each other thus they cannot separate macroscopically. So, due to incompatibility between the blocks microphase separation occurs which can form nanometer sized structures.

Even though electrospun fibers can be employed in a number of applications, the development of internal structures in electrospun fibers could significantly expand their applications; examples include sustained drug release, photonic fibers, and multifunctional textiles. Electrospinning of block copolymers offers an effective way to form internally structured fibers [7].

In the field of contemporary macromolecular science a great amount of research is being carried out in block copolymers. Controlling the size, shape and periodicity of

the nanoscale micro domains is needed to realize the nanoscale systems. It is said that as the progress is rapidly increasing in these areas, now the block copolymers stand on the verge of a new generation of sophisticated materials applications. In these applications nanostructures will play an important role [10].

## 1.2.1 Why Block Co-Polymers?

Block copolymers are the pre-eminent self-assembling materials because of [10]:

- By simply changing molecular weight, monomer structure and temperature the domain dimensions of the microstructures can be varied from 5-50 nm approximately.

- There are four different equilibrium symmetries in the bulk: lamellae, hexagonally packed cylinders, bicontinuous cubic double gyroid and body-centered cubic arrays of spherical micelles. Depending on the copolymer molecular weight, the volume fractions of the blocks and the interaction parameter between the respective monomers one of these periodic microphase-separated morphologies can be obtained.

- Any polymer can be selected for each of the blocks. Thus, it allows for each block to have properties tailored for desired applications.

- As the block copolymers contain different block thus different properties can be etched in like porosity. By removing one of the blocks porous fibers of

the other block can be obtained. Mesoporous carbon has been prepared by pyrolysis of poly(acrylonitrile-b-methyl methacrylate) diblock copolymer [11].

Over many years different block copolymers have been used to form films and fibers which are then used in different applications based on their properties. The ability of the block copolymers to form a variety of periodic patterns offers the potential to fabricate high density arrays which in turn can be used in data storage, electronics, molecular separation, DNA screening etc. Many researchers at Toshiba are also looking into the alignment of confined structures to produce patterned media for magnetic data storage application. Block copolymer domains can also be used as 'nanoreactors' to synthesize inorganic nanoparticles [12]. One of the potential uses of block copolymers is in producing porous nanostructures. Since there is intrinsic difference between the micro phase separated polymer blocks they may have different etch resistances to solvent or radiation which results in nanoporous structures. These can further be used in microfiltration or as a template to produce a wide range of functional materials [13]. Sometimes to improve the long range order in bulk samples electric field alignment has been successfully used [14]. Electrospinning of block copolymers has emerged as a novel way to form internally structured fibers[7]. Large surface area, controllable porosity, improved mechanical properties and flexibility in surface functionalization gives block copolymer nanofibers a platform for application in membrane and composite applications[15], biological applications[17], biomedical applications[18], optical and electrical

applications[16] and superhydrophobic surfaces[19,20]. Functionalized block copolymers are being used to immobilize bioactive molecules for drug delivery applications. Block copolymers can be prepared from various types of macroinitiators. PEG-b-PS and PS-b-PPG are amphiphilic block copolymers in nature which have been of great interest for the scientist for decades. A. Alh et al. [17] prepared macro azoinitiators by using PPG with primary amine ends. Electrospinning of these -NH$_2$ functionalized block copolymer was carried out in DMF solution. The same solution was used to prepare cast films and it was observed that the hydrophilic property increased in electrospun fibers as there was more penetration of water through fibers due to increased surface area. The electrospun nanofibers of PF-b-PNIPAAm-b-PNMA(polyfluorene-block-poly(N-isopropylacrylamide)-block-poly(N-methylolacrylamide) triblock copolymer were prepared which showed wettability and reversible on/off transition on photoluminescence as the temperatures varied [21]. PF block was designed for fluorescent probing, PNIPAAm block was designed for hydrophilic thermo-response and PNMA block was designed for chemical cross linking. The high surface area to volume ratio of the fibers enhanced the sensitivity and responsive speed to temperature. Electrospinning of PLA (polylactic acid) with PLGA poly (lactide-co-glycolide) random copolymers, PLA-b-PEG-b-PLA tri-block copolymer and Lactide[22] produces scaffolds which can be employed in cell storage and delivery. Core-Sheath structure was formed in electrospun nanofibers from polymer blends [23]. It was also shown that thermodynamic and kinetic factors affect the formation of these core-sheath structures. Novel micro-domain morphologies and defect-free

long-range ordering of the micro-domains can be created by combining block copolymer self-assembly with electrospinning. PEG (polyethylene glycol) and PCL (poly (ε-caprolactone)) are biodegradable and biocompatible polymers which can be used in biomedical field. PEG constitutes the soft hydrophilic segment while PCL constitute the hard hydrophobic segment. Electrospun nanofibers of PEG-b-PCL di-block copolymer were formed in dichloromethane solvent [24]. SEM (Scanning Electron Microscope) was used to analyze the microstructure of the formed electrospun fiber mats. It was shown that thicker fibers were obtained as the molecular weight of PEG block increased. Wetting behavior of PS-b-PNIPAM-b-PS (polystyrene-block-poly(N-isopropylacrylamide)-block-polystyrene) in aqueous environment was studied[25]. Hydrogel fibers can be formed for application in tissue engineering and to enhance material properties. Elastomeric nanofibers of styrene-butadiene-styrene tri-block copolymer were prepared from the solution of BCP and THF (tetrahydrofuran) and DMF (dimethylformamide) [26]. DMF was seen to improve the stability of the solution. SBS is a microphase-separated thermoelastomer. As the PS concentration increased it was observed that the morphology changed from spherical to cylindrical and lamellar domains.

## 1.3 Objective and Layout

Here, we introduce the formation of PS-b-PMMA (polystyrene-block-poly (methylmethacrylate)) nanofibers through the process of electrospinning and then inducing porosity in them by phase separation and then etching out one phase. Until now no studies have been carried out on the fabrication of PS-b-PMMA nanofibers and their characterization. This study can result in revealing the advantageous

properties of these nanofibers for different applications like in superhydrophobic and antireflective coatings.

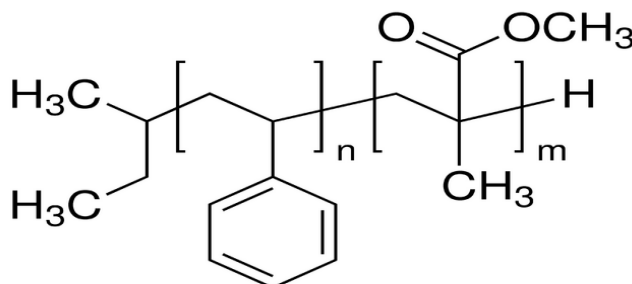**Chemical Name:-**PS-b-PMMA (polystyrene-b-poly (methyl methacrylate))



**Fig 1.1: Chemical Structure of PS-b-PMMA**

Two block copolymer of different molecular weights were used

1.  $M_n$ for PS: 57,000 g/mol

    $M_n$ for PMMA: 25,000 g/mol

    $M_w/M_n$: 1.07

2.  $M_n$ for PS: 96,500 g/mol

    $M_n$ for PMMA: 36,500 g/mol

    $M_w/M_n$: 1.11

**Properties-** The PS-b-PMMA di-block copolymer is thermally stable. The blocks PS and PMMA have high interaction energy due to which they easily micro phase separate in order to minimize free energy of the system and form ordered morphologies with nanometer scale dimensions. Both the blocks individually provide certain characteristics like PS is a stiff material having resistance to acids and is also chemically inert. PMMA is also a tough and rigid plastic with low UV

resistivity. This block copolymer has attracted a great deal of interest in nano-technological applications.

In Chapter 2, we have introduced the synthesis of PS-b-PMMA nanofibers through electrospinning and optimized the parameters for the same in terms of processing and solution parameters. The effect of changing parameters was observed with the help of SEM imaging. Characterization for BCP fibers and powder was done in terms of FTIR and TGA. In Chapter 3 we have further explored the properties of these electrospun nanofibers. We studied their wettability characteristics to learn about their wetting nature in terms of contact angle. Further we also did reflectance measurement for these fibers/ beaded fibers. Absorbance studies were carried out studying the effect of changing time, temperature and concentration of adsorbate.

# Chapter 2

# Fabrication of PS-b-PMMA Derived Electrospun Nanofibers

## 2.1 Materials

Two different block co-polymers PS (57,000)-PMMA (25,000) ($M_w$/ $M_n$=1.07) and PS (96,500)-PMMA (35,500) ($M_w$/ $M_n$=1.11) were purchased from Polymer Source, Inc., Canada and were used as such. N, N-Dimethylformamide ($C_3H_7NO$) (DMF) was purchased from S D Fine-Chem Limited (SDFCL), India. Reagents like acetic acid (99.7%) and acetone were also purchased from Alfa Aesar, India and Sigma Aldrich, India respectively and used as such. Double-distilled water was used throughout the experiments.

## 2.2 Method

### 2.2.1 Preparation of polymer solution for electrospinning

The solution of PS-b-PMMA was prepared in DMF solvent. Two different concentrations (8 wt% and 16 wt%) were used in the experiments. The solutions were stirred and heated at 35°C until they become clear and transparent. The solutions were cooled prior to electrospinning.

### 2.2.2 Electrospinning

The basic electrospinning setup (Fig 2.1) cons+ists of three major components which includes a syringe needle also called the spinneret, a high voltage power

supply (an assembly which has been attached to an infusion pump) and a metallic plate which acts as a conductive collector, which is grounded. Initially, the charged polymer solution is fed through the spinneret and electric field is applied which forms a suspended droplet at the orifice. At this instance the surface tension of the droplet is in equilibrium with the applied electric field. Now, as the electric field is increased then after a threshold value it overcomes the surface tension of the droplet at the orifice. As a result of the electrostatic repulsions of the surface charges in the polymer droplet a Taylor cone is formed. A tiny jet is ejected at this point from the surface of the droplet and is drawn towards the collecting plate. As the jet emerges from the spinneret it undergoes instabilities known as Rayleigh instability which leads to the bending and whipping motion and thus the fibers are elongated in turn decreasing in diameter. As the process proceeds the solvent from the jet of the polymer solution evaporates giving rise to dry and ultrathin fibers [27,12]. Thus, the product obtained on the collector is non-woven fibrous scaffolds with large surface area to volume ratio.

Three major forces combine and determine the final morphology of the fibers. Surface tension tends to minimize the surface energy by converting the liquid jet into spherical droplets. Electrostatic repulsions interplays to increase the surface area of the product by favoring the formation of jets rather than beads. Viscoelastic forces resist the rapid changes in the shape.

The prepared solution was taken in a 2 mL syringe fitted with a metallic needle. The flow rate, applied voltage and tip to collector distance were ranged between 3-5µl/min, 10-22 kV and 6-10 cm respectively. Si wafer was used as substrate to

collect the formed fibers. The same electrospinning conditions were varied for both the high molecular weight and low molecular weight PS-b-PMMA block copolymer.
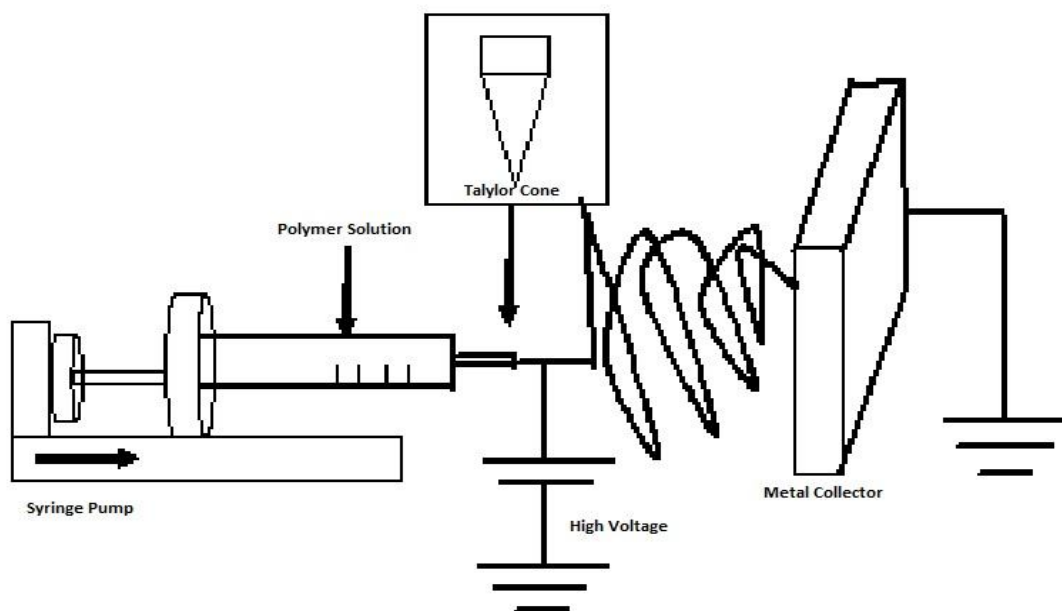


**Fig 2.1: Basic setup of an electrospinning apparatus**

## 2.2.3 Annealing and Etching

In order to generate porosity and in turn to yield different morphology the as-spun samples were further treated. They were annealed (thermal and solvent annealing) which imparts an increase in chain mobility thereby causing phase separation. Thermal annealing was carried out in vaccum at 165°C for a duration of 12 hours. Solvent annealing was proceeded with acetone vapours which are PMMA selective for different time lengths varying from 2 minutes to 12 hours. So, consecutively the effect of changing solvent annealing time was observed. Then these annealed samples were UV exposed (wavelength- 254 nm) for a period of 2 minutes. UV exposure crosslinks the PS phase whereas degrades the PMMA phase. Acetic acid

washing followed by DI water washing for 30 seconds each results in the removal of degraded PMMA phase thus generating porosity in the PS nanofibers. Table 2.1 shows all the steps which have been followed to carry out the required experiments.

**Table 2.1: Enlisting of all the experimental steps**

| Process | Conditions |
|---|---|
| Solution Preparation | PS-b-PMMA solution in DMF (Dimethylformamide) by varying solution concentration from 8 wt% to 16 wt% |
| Electrospinning | Electrodes separation: 6 cm – 10 cm<br><br>Flow rate: 3 μl/min – 5 μl/min<br><br>Applied Voltage: 10 kV – 22 kV |
| Thermal Annealing | At 165°C in vaccum for 12 hours |
| Solvent Annealing | In acetone vapor for different time lengths |
| UV Exposure | 2 minutes |
| Etching | Washing with Acetic Acid and DI Water for 30 seconds each |

## 2.3 Characterization

### 2.3.1 SEM Analysis

**Method-** The obtained fibers from the experiments were characterized by SEM (Scanning Electron Microscope) imaging. SEM produces images of a sample by scanning it with a focused beam of electrons. The electrons interact with the atoms of the sample which produces signals that can be detected and provides the

information about the surface's topology and composition [31]. Morphologies of the obtained non-woven mat deposited on Si wafer (1 cm x 1 cm) substrate was investigated using the Scanning Electron Microscope (SEM) (Phenom World, Pro X) imaging operated at 5 kV.

**Results-** Morphologies of the obtained non-woven mats and cast films were observed with the help of SEM imaging. The effect on the fibers morphology by tuning the electrospinning parameters was studied (Fig. 2.2). The applied electric field affects the thinning of the jet. It was observed that as the voltage increased from 15 kV to 18 kV (Fig. 2.2a- b), keeping the distance of 10 cm between the electrodes, the morphology changed from spherical to spindle-like and the density of beads decreased as can be seen. As the applied voltage is increased the electrostatic repulsive force on fluid jet increases thus favouring the formation of fibers. The distance between the electrodes should be optimum as to allow the complete evaporation of the solvent. For every polymer-solvent system there is an optimum range of electric field applied within which the fiber formation occurs and beyond it beaded morphology is seen as the droplet volume decreases giving rise to bead formation [30]. Thus, it was observed that on further increasing the voltage to 20 kV (Fig. 2.2c) there was more beads formation. Thus, the applied voltage was set to 18 kV. Next, the flow rate needs to be optimized to maintain the shape of the taylor cone and to replace the solution that is lost when jet is ejected. As the flow rate for 8wt% solution is increased from 3 µl/min to 5 µl/min (Fig. 2.2d – f) while maintaining the applied voltage at 18 kV and the electrode separation of 10 cm it could be seen that beaded morphology at 3 µl/min (Fig. 2.2d) changes to beaded fibers at 5 µl/min(Fig. 2.2f). For a given voltage a corresponding feed rate is

required to maintain a stable taylor cone and in this case it was set to 5 µl/min. The viscosity of the solution is related to the polymer concentration and tuning of viscosity in turn affects the resultant morphology of the fibrous mats. As the concentration was worked upon it was observed that at a lower concentration of 8wt% (Fig. 2.2g), beaded morphology was obtained as the charged jet fragments into discrete droplets before reaching the collector. As the concentration is increased to 12wt% (Fig. 2.2h) and then further to 16wt% (Fig. 2.2i) the chain entanglement improves and nanofibers are obtained and density of beads decreases as can be observed from Fig 2.2g-i. The other condition which was worked upon was the needle diameter for a solution concentration of 16wt%, applied voltage of 18 kV with a flow rate of 5 µl/min and electrode separation of 10 cm. Depending on the viscosity of the solution or 21 gauge needle (inner diameter = 0.80 mm) (Fig. 2.2j) the needle was getting clogged and it was difficult to get continuous fibers. As the needle diameter was increased to 0.90 mm for a 20 gauge needle (Fig. 2.2k) the fibers obtained were continuous and uniform. Further increasing the needle diameter to 1.20 mm i.e. 18 gauge (Fig 2.2l) it was seen that all the solution was depositing on the collector in droplets form.
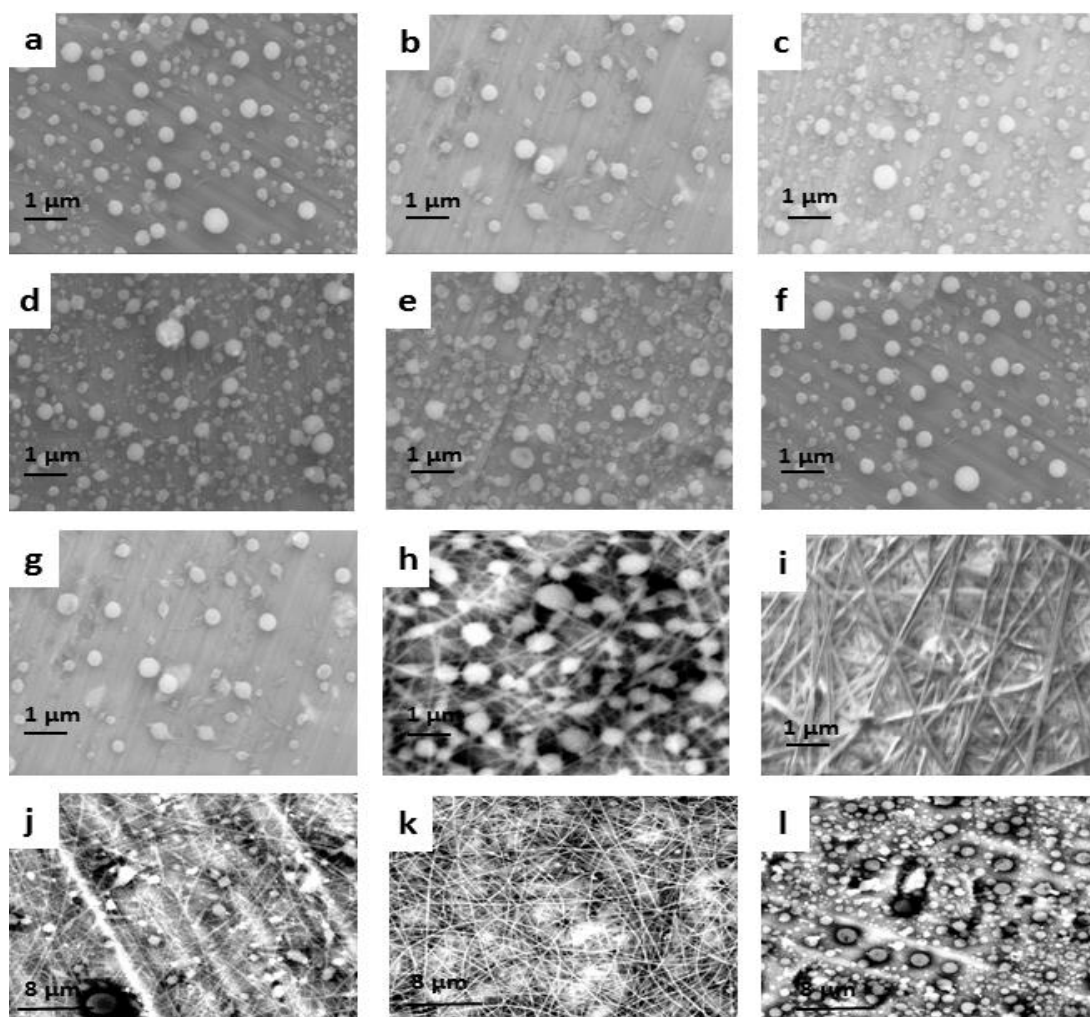
**Fig 2.2: SEM images- samples obtained with different morphologies by changing the process parameters like electric field(a-c) (a) 15 kV ,(b) 18 kV and (c) 22 kV; flow rate(d-f) (d) 3 µl/min ,(e) 4 µl/min and (f) 5 µl/min; concentration(g-i) (g) 8 wt% ,(h) 12 wt% and (i) 16 wt%; and needle gauge(j-l) (j) 21 gauge ,(k) 20 gauge and (l) 18 gauge**

All these conditions were optimized for both the block copolymers and thus the effect of changing the molecular weight was also observed. The molecular weight affects the entanglement of the polymer chains present in the solution and in turn the solution viscosity. The entanglement of chains prevents the jet from breaking up and thus maintains a continuous solution jet. For higher molecular weight nanofibers can be obtained at a much lower solution concentration. Finally, the optimized

parameters as shown in Fig. 2.3 which resulted in for lower block copolymer (Fig. 2.3a – b) were 16 wt% solution concentration was electrospun with optimum distance between the electrodes set as 10 cm with a flow rate of 5 µl/min at an applied voltage of 18 kV and 20 gauge (0.90 mm dia) syringe needle and the scaffold showing fibrous morphology with minimum density of beads. Whereas for higher molecular weight polymer (Fig. 2.3c – d) the optimized parameters were showing long, continuous fibers for 12 wt% solution with working parameters of 10 cm electrode separation, applied voltage of 18 kV and the flow rate of 3 µl/min. The needle syringe in this case was 24 gauge (0.55 mm dia).



**Mol. Wt. PS(57k)-b-PMMA(25k)**
Concentration: 16 wt%
Needle Gauge: 20 gauge
Applied Voltage: 18 kV
Electrode Separation: 10 cm
Flow Rate: 5 µl/min

**Mol. Wt.PS(96.5k)-b-PMMA(35.5k)**
Concentration: 12 wt%
Needle Gauge: 24 gauge
Applied Voltage: 18 kV
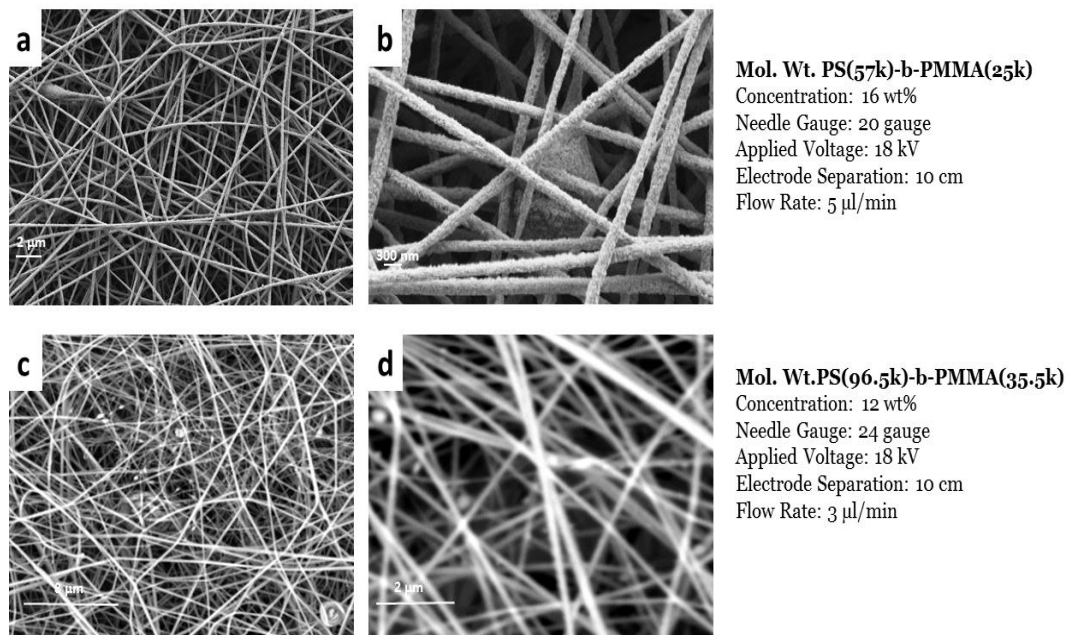Electrode Separation: 10 cm
Flow Rate: 3 µl/min

**Fig 2.3: SEM images showing the optimized conditions for electrospinning for Electrospun PS-b-PMMA (a,b) beaded fibers; (c,d) nanofibers**

For inducing the porosity the thermal annealed samples (Fig. 2.4a) showed that the fiber morphology was not retained. As the annealing was carried out at a temperature of 165°C, which is much above the glass transition temperature of the two blocks PS ($T_g$ = 90°C) and PMMA ($T_g$ = 105°C), both the blocks phase

separated and melted and no fibers were retained as seen in the Fig. 2.4a. Fig. 2.4b clearly depicts that even though the morphology was not retained yet porosity has been achieved after washing the annealed and UV exposed samples with acetic acid and DI water. High magnification inset image in Fig 2.4b shows the fine distribution of the pores in the melted film.
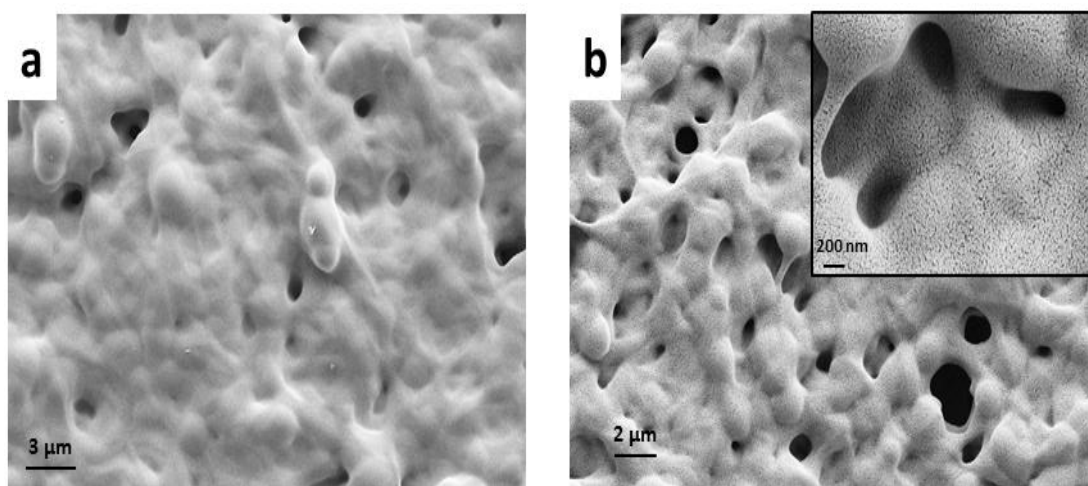


**Fig 2.4: FESEM images of Electrospun PS-b-PMMA fibers after a) thermal annealing and b) after etching (Inset showing higher magnification image)**

As the thermal annealing was not helpful in keeping the morphology of the fibers intact, solvent annealing was carried out at different time lengths varying from 2 minutes to 12 hours. It was observed that at 2 minutes (Fig. 2.5a) and 5 minutes (Fig. 2.5b) the fiber morphology could be maintained intact. As the annealing time was increased to 10 minutes (Fig. 2.5c) it was observed that the fibers had almost lost their morphology and after a duration of 12 hours they have completely been melted as in thermal annealing case and have lost their integrity. Solvent vapour assisted annealing helps in lowering the glass transition temperature ($T_g$) of the blocks present and helps in their phase separation at a much lower temperature [32].

Later the samples were UV exposed to crosslink the PS phase and simultaneously in order to degrade the PMMA phase they were etched which resulted in porosity in the samples. Fig. 2.5d – f shows the etched samples with fine porosity implying that degraded phase has been removed generating porosity.
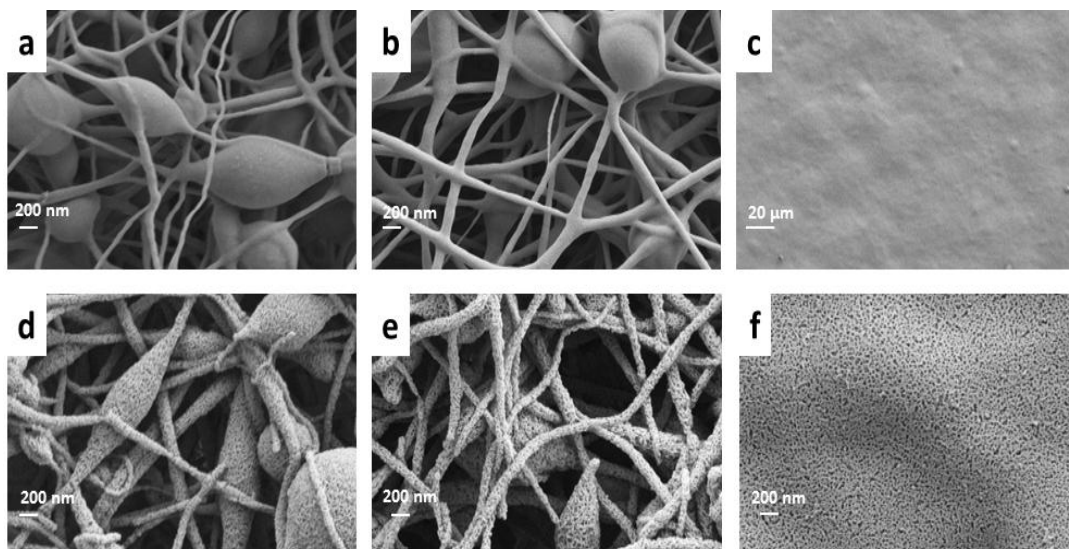


**Fig 2.5: FESEM images of Electrospun PS-b-PMMA fibers after solvent vapor assisted annealing (a-c) and etching (d-f) by changing annealing time as (a,d) 2 minutes, (b,e) 5 minutes and (c,f) 10 minutes**

## 2.3.2 FTIR

**Method:** This is the analytical technique used to qualify and quantify compounds utilizing infrared absorption of molecules. Absorption occurs when the energy of the beam of the light (photons) are transferred to the molecule. The molecule gets excited and moves to a higher energy state. The energy transfer takes place in the form of electron ring shifts, molecular bond vibrations, rotations and translations. IR is mostly concerned with vibrations and stretching. A molecule is infrared active if it possesses modes of vibration that cause a change in dipole moment. A detector

registers how much light is transmitted through the sample. The result is a characteristic spectrum showing the transmittance of electromagnetic radiation as function of wavelength. Different functional groups absorbed different energy's [33]. A FTIR (Bruker, Tensor 37), equipped with the Universal ATR Sampling Accessory was used to obtain spectra in the 1000 - 3500 $cm^{-1}$ region (Transmittance vs. wavenumbers mode) at room temperature and humidity.

**Results:** Fig 2.6 shows an FTIR spectrum for the PS-b-PMMA nanofibers produced by the electrospinning method. These results shows the various groups present in the fibers which can be correlated to the groups present in the block copolymer (Fig 3.5 (inset)). The C=O at 1732 $cm^{-1}$ and C-O stretch at 1147 $cm^{-1}$ can be related to the ketonic group present in the PMMA block. The aromatic group present in the PS phase can be seen as C=C stretch at a wavelength of 1448 $cm^{-1}$ in the FTIR plot [34].
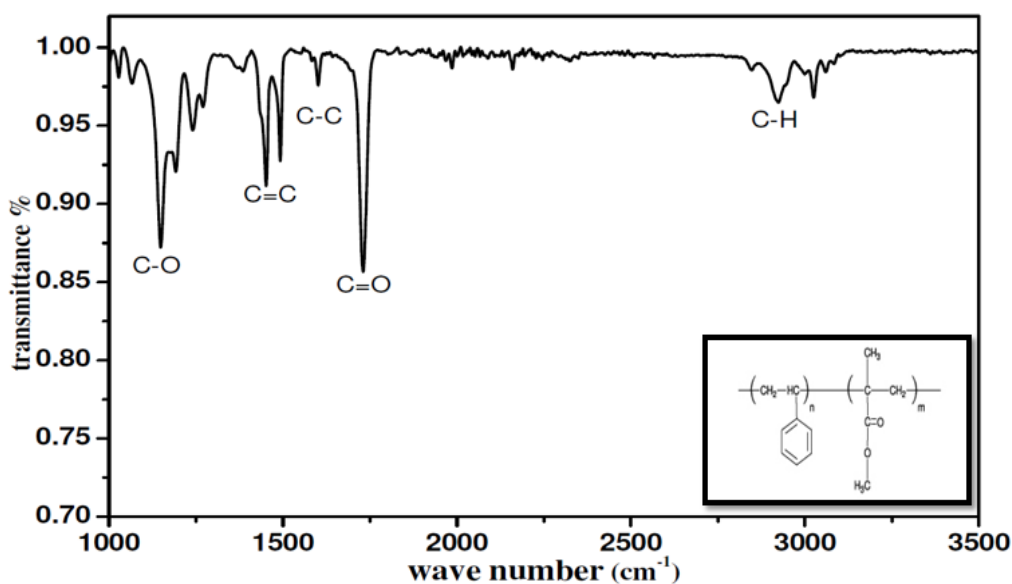


**Fig 2.6: FTIR Spectrum (Inset depicts different groups present in (PS-b-PMMA))**

### 2.3.3 TGA

**Method:** TGA detects the amount and rate of change in the mass of a sample as a function of temperature or time in a controlled atmosphere. Thermogravimetric analysis (TGA) (Perkin Elmer Pyris 1 TGA) of the as-spun fibers and block copolymers was carried out using a under helium atmosphere (30 ml/min) at a heating rate of 5°C/min from room temperature (40°C) to 500°C.
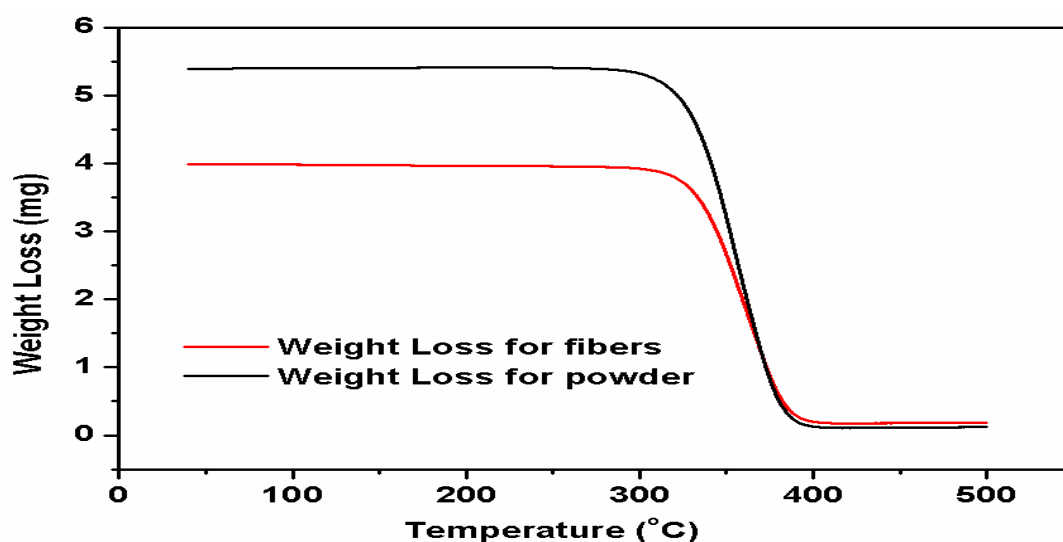
**Results:**



**Fig 2.7: TGA analysis for PS-b-PMMA powder and fibers**

The graphs show that the block copolymer powder and in fibrous form starts to lose its weight between 250°C to 300°C. In case of BCP powder (Fig 2.7) it gradually loses its weight from 5.39 mg to 0.17 mg and after 400°C it again becomes constant. For BCP fibers (Fig 2.7) it starts losing its weight at 290°C from 3.98 mg to 0.21 mg and again after 400°C the weight becomes constant. This shows that the integrity and the properties of the PS-b-PMMA block copolymer was retained even after it was spun into fibers.

23

# Chapter 3

# Properties of PS-b-PMMA Derived Electrospun Nanofibers

## 3.1 Wettability characteristics

**Method:** Wettability of a surface can be measured by contact angle. When a water drop is deposited on a planar solid surface, the angle between the outline tangent of the drop at the contact location and the solid surface is called contact angle ($\theta$). The contact angle is a measure of the ability of a liquid to spread on a surface.

**Hydrophobic (Water Hating)** $-$ Surface which repels water is termed as hydrophobic and contact angle of such surface is greater than 90°.

**Hydrophilic (Water Loving)** $-$ Surface which attracts water is termed as hydrophilic and contact angle for such surface is less than 90°.

**Super hydrophobic** - Surfaces which have contact angle greater than $150^0$.

Contact angle of water was measured on solution cast films and electrospun films. Contact angles were measured by goniometer (Ramé-hart instrument co., Model 290 F4 series) by image processing of sessile drop with a DROPImage Advanced software. Drops of purified water, 3 µl, were deposited on the surface to form sessile drop using a micro-syringe attached to the goniometer. Contact angles on different parts of films were measured and averaged.

**Result:** The contact angle measurements reveal the surface characteristics in terms of wettability. As being depicted in Fig 3.1, the as-spun fibers of lower molecular weight polymer and high molecular weight polymer showed ultra-hydrophobicity with a contact angle of 129.7 $\pm$ 3.2$^o$. The thin film, prepared by spin coating for comparison purpose, showed relatively less contact angle around 118.2 $\pm$ 2.6$^o$. The thermally and solvent annealed samples showed contact angle of 84.8 $\pm$ 3.9$^o$ and 85.7 $\pm$ 2.7$^o$ respectively which decreased to 71.7 $\pm$ 4.5$^o$ after UV exposure as a result of increased surface energy. This contact angle was again seen to increase to 88.9 $\pm$ 3.9$^o$ after etching suggesting the removal of PMMA phase. Same trend was observed in films treated for phase separation. Consecutively the films showed less contact angle in comparison to the fibrous matrix. Transition of wettability from hydrophilic to hydrophobic can be observed by changing the morphology of the fibrous mat.
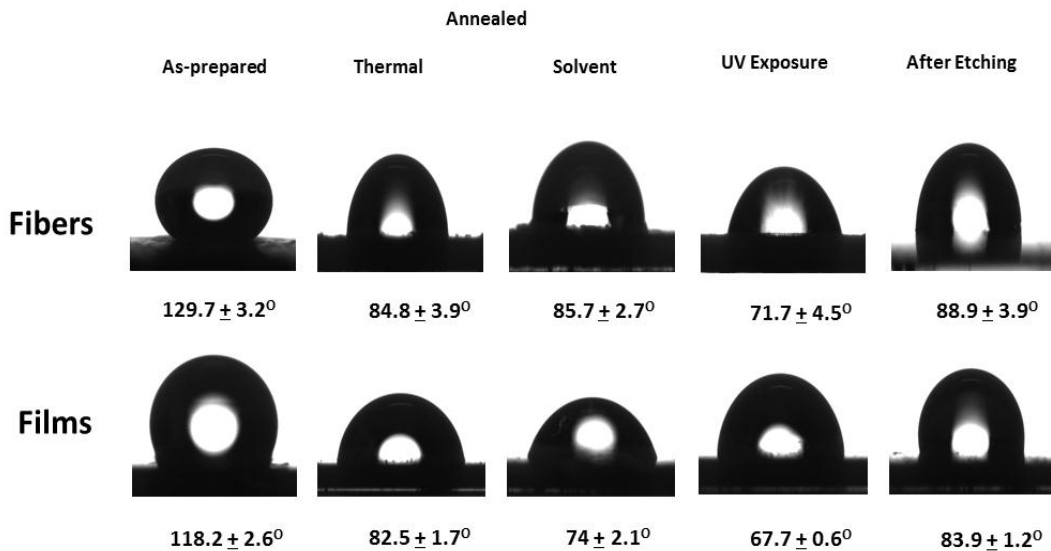


**Fig 3.1: Contact angle of fibers and films for as-spun, annealed, UV exposed and etched samples**

## 3.2 Reflectance Measurement

**Method:** In simple terms an antireflective (AR) coating is applied to surfaces to reduce reflection which in turn improves the efficiency of the system since only a little part of light is lost. The principle of an AR coating is based on the destructive interference of reflected light from in between the interfaces. AR coating in the visible and near infrared spectrum (400 nm – 2000 nm) effectively enhances the transmittance of light through an optical surface and reduce glare to obtain a clear and bright view of images and achieve high power conversion efficiency for solar cells. It finds its application in car dashboards, computer screens and solar cells. Reflective surfaces having high refractive index with respect to the air medium results in higher reflectivity i.e. more the refractive index more the reflection. Fresnal equation is used to calculate the reflection at normal angle of incidence between two mediums of refractive index n1 and n2.

$$r = \left(\frac{n1 \sim n2}{n1 + n2}\right)^2$$

It is clear from the above equation that larger the difference between the refractive indices of the two mediums, the greater will be the reflection of light.

Visible Range of light lies between 380 – 780 nm whereas Ultraviolet (UV) and Near-Infrared Radiations (NIR) are located below and above the visible region range respectively. A UV-VIS spectrophotometer (PerkinElmer, Lambda 35) was used to measure the optical properties in regard of reflectance of the sample prepared in the range of 400 nm to 800 nm (angle of incidence- 45 deg). In the next step keeping the

wavelength of the light constant for all samples the angle of incidence was varied from 15º to 75º.

**Results:** According to the literature the refractive index of the block copolymer PS-PMMA[28], the polymer PS[29] and the polymer PMMA[29] are 1.49, 1.59 and 1.489 respectively. Reflectance studies (Fig. 3.2) showed that in the visible region the least reflectance is shown by the etched samples and then fibers and then beaded fibers. While after the porosity has been developed the reflectance value increases. It gives us an idea that as the PMMA phase has been removed only PS phase remains so the refractive index of the polymer increases thus causing an increase in the value of the reflectance. The nanofibers of this block copolymer hence can be used for antireflective coatings.
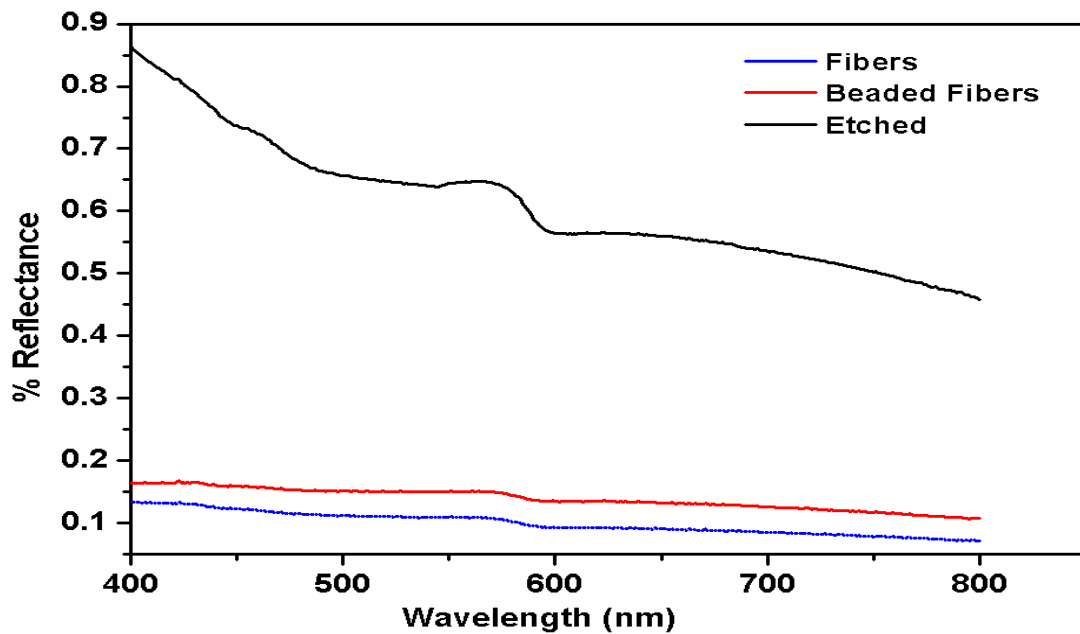


**Fig 3.2: Wavelength vs %Reflectance of Fibers, Beaded fibers and Etched samples from 400 nm to 800 nm with angle of incidence = 45deg**

The as-spun fibers or beaded fibers showed more reflectance as compared to the film of the same block copolymer (Fig 3.3). As the wavelength was fixed and the angle of incidence was varied from 15º to 75º (Fig 3.4) again same trend was observed that films (Fig 3.4(a)) showed less reflectance as compared to as-spun fibers (Fig 3.4(b)) confirming that for anti-reflectivity coatings films will serve as a better option. As the angle of incidence increases the reflectance for both film and fibers decreases upto 65º and after that the trend changes as the reflectance of film is greater that reflectance of fibers. This suggests that at angle of incidences greater than 65º fibers are showing more anti-reflectivity than films.
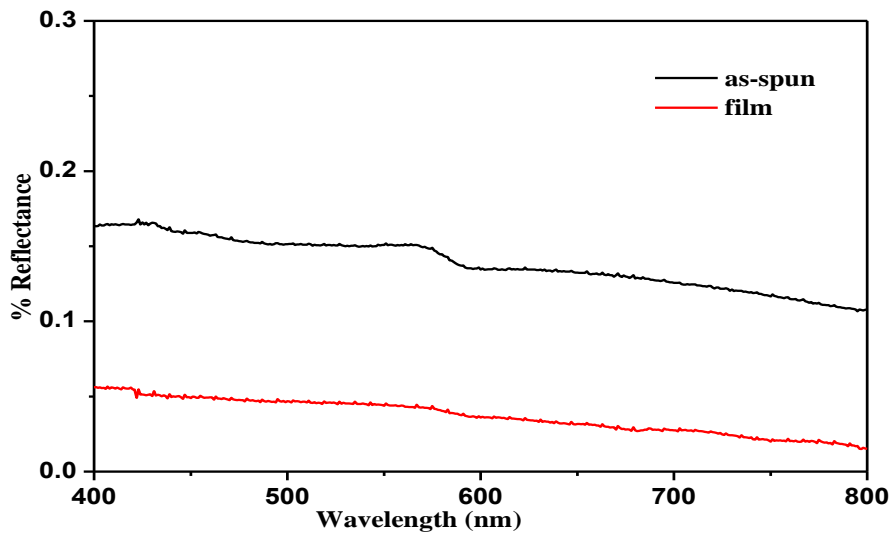


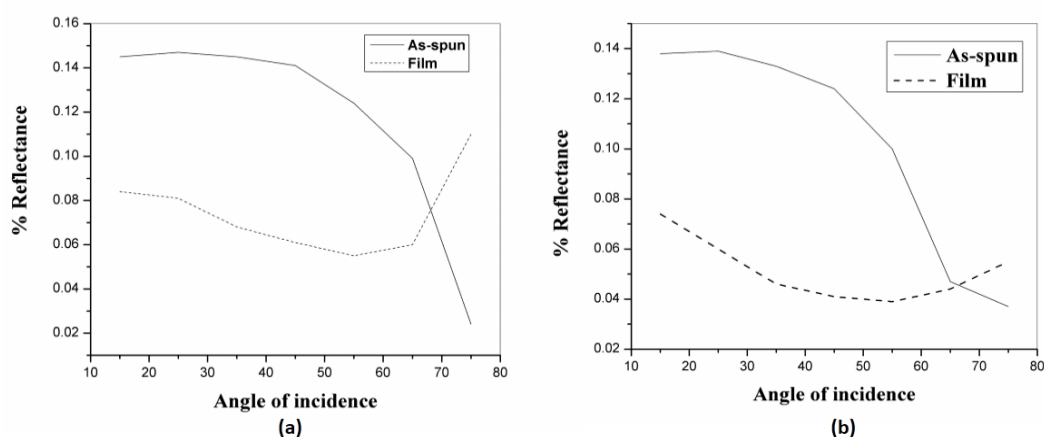**Fig 3.3: Graph showing reflectance of as-spun and cast film**

**Fig 3.4: Graph showing reflectance vs angle of incidence at fixed wavelength of (a) 450 nm and (b) 700 nm**

## 3.3 Adsorption Characteristics

Textile industries release large quantities of dyes into the surroundings which possess serious environmental problems. Most of the dyes during the dyeing process are lost as liquid effluents. Removing color from theses dyes is a requirement and a problem faced by textile and dye manufacturing industries. Methylene blue is a cationic dye used in dye, paint production, diagnostics, microbiology and surgery [35]. Many methods coagulation, floatation, chemical oxidation, adsorption and solvent extraction have been used to remove color from wastewater [36, 37]. Adsorption methods, out of all these, has been found to be most effective in treating dye-containing effluents [35, 38].

Methylene Blue purchased from Alfa Aesar, India was used as a dye and its solution was prepared in DI water. ACF fabric and PS-b-PMMA fibers deposited on these

fabrics were used to study the adsorption characteristics. A UV-VIS spectrophotometer (PerkinElmer, Lambda 35) was used for absorbance measurements. A stock solution of 20 mg/l or 20 ppm was prepared and then it was further diluted to prepare respective solutions of 5 ppm, 15 ppm and 20 ppm. Adsorption studies were carried out by studying the effect of changing time, temperature and concentration of adsorbate.

## 3.3.1 Effect of change in concentration of adsorbate and time

**Method:** A standard plot was first plotted for all the solutions prepared (5 ppm- 20 ppm). Then for each of the solutions the time was varied as 5 min, 10 min, 15 min, 60 min, 120 min, 240 min, 360 min, 720 min and 1440 min. ACF fabric of fixed dimensions (2 cm * 2cm) was used throughout. PS-b-PMMA fibers were deposited on these fabrics for a fixed time period of 30 min to confirm the uniformity in amount of deposition. Then, these fabrics were immersed into a specific solution for a specific time period and then the absorbance of the left solution was measured.

**Results:** The solutions showed maximum absorbance around 664 nm. This peak was considered to plot a standard curve (Fig 3.5) for all the varying concentrations. The curve showed a linear relation between concentration and absorbance.
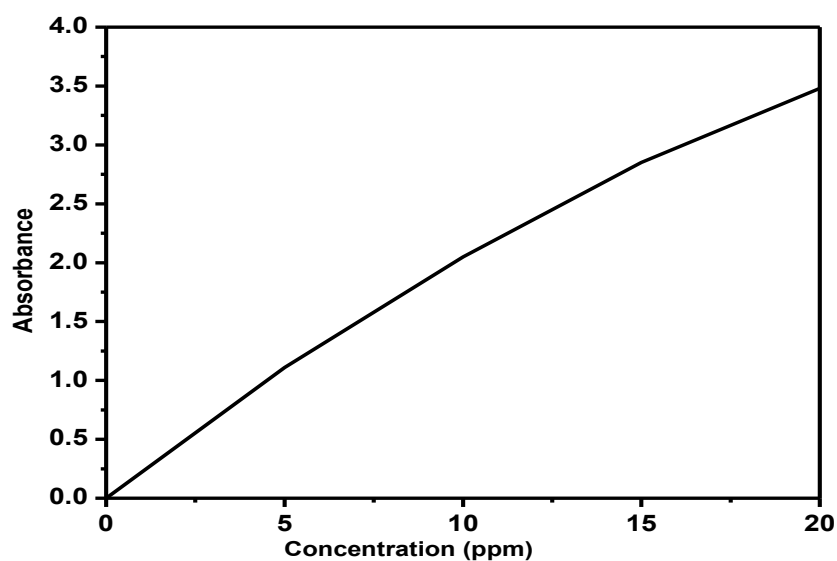
**Fig 3.5: Standard curve of Absorbance vs Concentration**

Now, for ACF fabrics (Fig 3.6 (a)) as the time was increased it was observed that the %adsorption also increases for every concentration. But as the concentration increases from 5 ppm to 20 ppm the %adsorption shows a decrease from 81% to 62%. The considerable amount of increase in %adsorption with time signifies increase in adsorption capacity. For ACF+BCP (Fig 3.6(b)), the %adsorption is more in comparison to ACF fabric. The %adsorption for ACF+BCP decreases from 89% to 85% as the concentration is increased from 5 ppm to 20 ppm. As observed that the decrease in %adsorption as concentration increases for ACF+BCP is less as compared to ACF. In case of ACF there is a much higher decrease in %adsorption signifying that saturation is attained earlier.
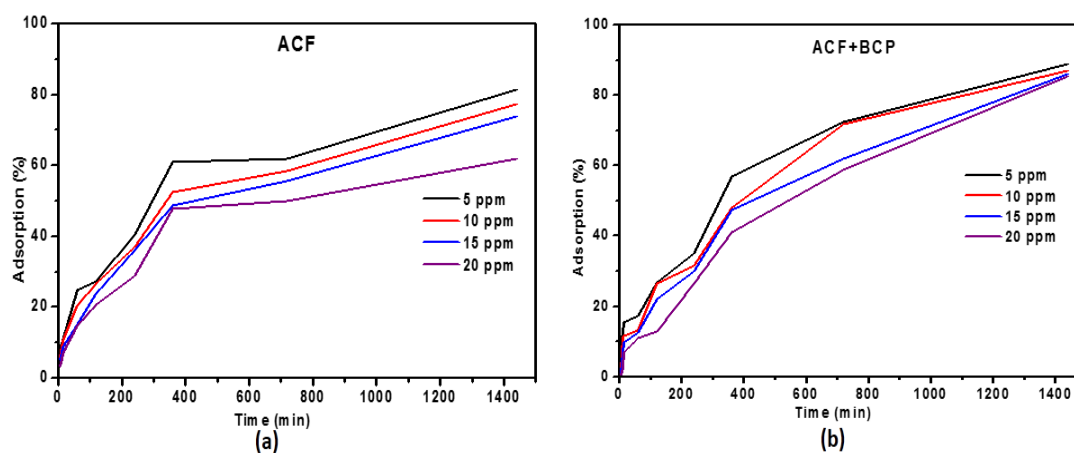
**Fig 3.6: %Adsorption vs Time for (a) ACF fabric and (b) fibers deposited on ACF fabric**

When concentration was kept constant and comparison was made between ACF fabric and ACF+BCP fabric it was observed that the %adsorption was higher for ACF+BCP. Due to increased surface area due to deposition of fibers on the ACF fabric the adsorption of methylene blue increases to a considerable extent. As can be seen for 5 ppm (Fig 3.7(a)) the %adsorption in case of ACF is 81% while for ACF+BCP it is 89%. Similarly, for constant concentration of 20 ppm (Fig 3.7(b)) the %adsorption for ACF is 62% while for ACF+BCP it is 85%. It can also be observed from both the graphs (Fig 3.7) that after 500 min i.e. 7-8 hours only the %adsorption for ACF+BCP shows an increase. Whereas before 500 min the %adsorption for ACF is more compared to ACF+BCP.
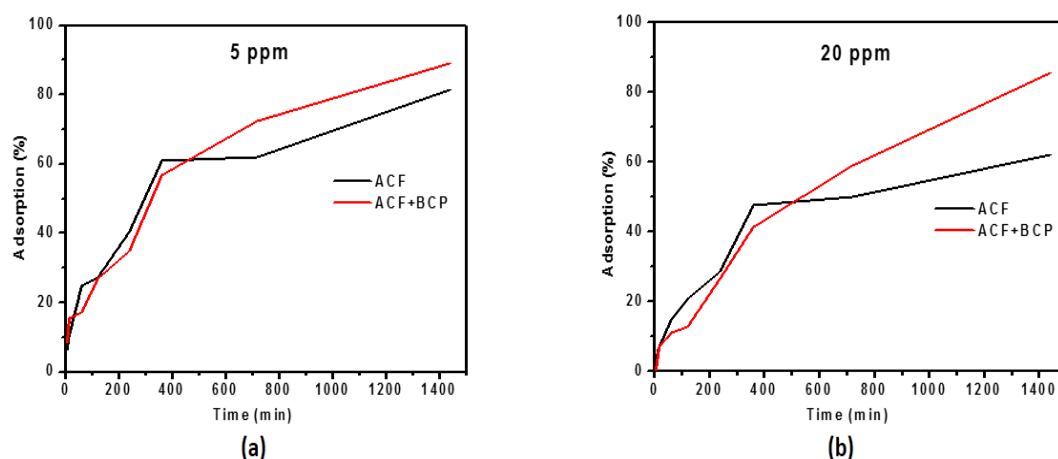
**Fig 3.7: Graphs showing %adsorption vs time for ACF and ACF+BCP at (a) 5ppm and (b) 20ppm**

## 3.3.2 Effect of change in temperature

**Method:** Keeping the concentration constant at 5 ppm the temperature was varied as 30ºC, 45ºC and 60ºC for varying time lengths of 30 min, 60 min, 120 min, 240 min, 720 min and 1440 min. This was carried out for both ACF fabric and fibers deposited on ACF fabric.

**Results:** It was observed that (Fig 3.8) as the temperature increases from room temperature to 60ºC the %adsorption increases to a greater extent. In the case of ACF (Fig 3.8 (a)) the %adsorption increased from 81% to 97% as the temperature was increased. While in the case for ACF+BCP (Fig 3.8(b)) the %adsorption was seen to increase from 89% to 98% on increasing the temperature.
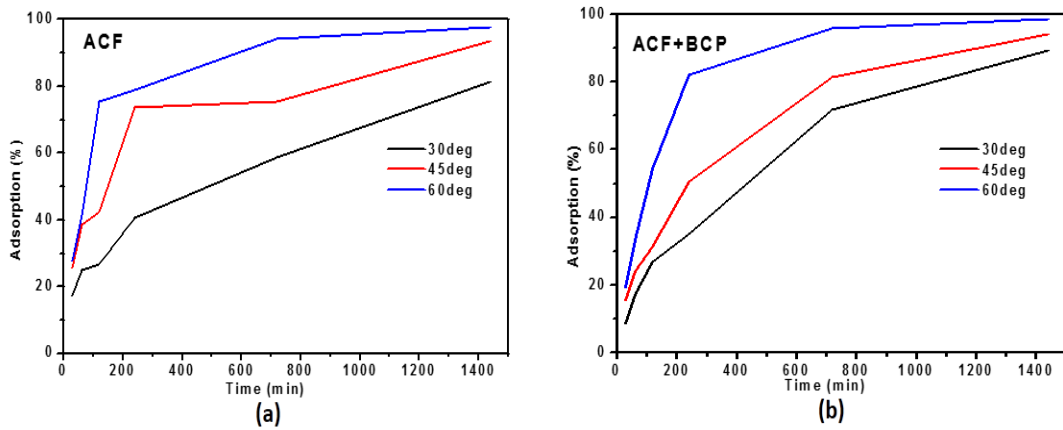
**Fig: Graphs showing %adsorption vs time at different temperatures for (a) ACF and (b) ACF+BCP. Adsorbate concentration= 5 ppm**

Keeping the concentration constant to 5 ppm at a constant temperature of 60 °C the %adsorption vs time was plotted for both ACF and ACF+BCP (Fig 3.9). As seen earlier the %adsorption for ACF+BCP was higher as compared to for ACF fabric.
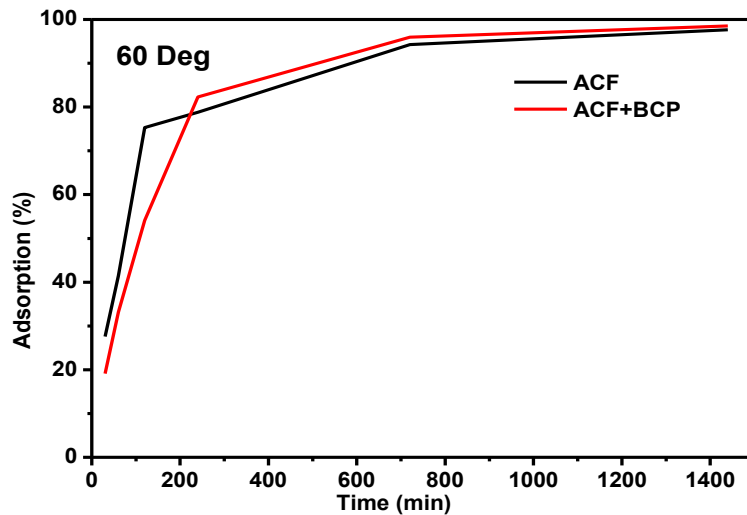


**Fig 3.9: %adsorption vs time for ACF and ACF+BCP for 5 ppm and 60 °C**

# Chapter 4
# Summary and Future Work

In this work we successfully optimized the electrospinning conditions for obtaining PS-b-PMMA beaded fibers and nanofibers and then carried out the structural analysis of the as-spun fibers by characterizing them by TGA and FTIR. Micro-phase separation was achieved by thermal annealing and solvent annealing followed by etching. This leads to porosity in electrospun nanofibers. The wettability studies showed that the highest contact angle was shown by as-spun fibers while 10 minutes solvent annealed samples after annealing and getting UV exposed showed the least contact angle. Thus, wettability was shown to be varying over a wide range from strong hydrophilic to ultra-hydrophobic by simply tailoring the morphology of electrospun PS-b-PMMA nanofibers. Reflectance studies carried out comparatively showed film to be more anti-reflective than fibers and etched samples. Further, the adsorption capacity showed an increase when fibers were deposited on ACF due to an increase in surface area. These studies reveal the use of these fibrous scaffolds in a number of applications like antireflective coating showing hydrophobic behavior and also for adsorption techniques.

Furthermore, these fibers can be pyrolyzed to obtain mesoporous carbon nanofibers which further can be used in filtration applications.

# References

1. Vibha, K.; Sergio, M.; Lee, J.H.; Huy, N.; Manuel, M.; Joo,Y.L. *Adv. Mater.* **2006**, 18, 3299–3303

2. Teo, W.E.; Ramakrishna, S. *Nanotechnology*, **2006**, 17, 89-106

3. Greiner,A.; Wendroff, J.H. *Angew. Chem. Int. Ed.*, **2007**, 46, 5670-5703

4. Demirel, G.B.; Buyukserin, F.; Morris, M.A.; Demirel, G. *Appl. Mater. Interfaces* **2012**, 4, 280-285

5. Thomassin, Jean-Michel; Debuigne, A.; Jérôme, C.; Detrembleur,C. *Polymer* **2010**, 51, 2965-2971

6. Bae, D.; Jeon, G.; Jinnai, H.; Huh, J.; Kim, J.K. *Macromolecules* **2013**

7. Ma, Minglin; Krikorian, Vahik; Yu, Jian H.; Thomas, Edwin L.; Rutledge, Gregory C. *Nano Lett.* Vol. 6, No. 12, **2006**, 2696-2972

8. Ramakrishna, S.; Fujihara, K.; Teo, W.E.; Yong, T.; Ma, Z.; Ramaseshan, R. *MaterialsToday* **2006**, 3, 40-50

9. Li, Z.; Wang, C. **2013**, 15-27

10. Lodge, Timothy P. *Macromol. Chem. Phys*. **2003**, 204, 265-273

11. Nguyen, Chi Thanh; Kim, Dong-Pyo. *J. Mater. Chem*., **2011**, 21, 14226-14230

12. Hamley, I W. *Nanotechnology*, **2003**, 14, 39-54

13. Zoelen, Wendy van; Brinke, Gerrrit ten *Soft Matter*, **2009**, 5, 1568-1582

14. Darling, S. B. *Prog. Polym. Sci*. **2007**, 32, 1152-1204

15. Yao, X.; Wang, Z.; Yang, Z.; Wang, Y. *J. Mater. Chem. A* **2013**, 1, 7100

16. Fasolka, M.J.; Mayes, A.M. *Annu. Rev. Mater. Res.* **2001**, 31, 323–355

17. Alli, Abdulkadir; Hazer, Baki; Menceloglu, Yusuf; Suzer, Sefik *European Polymer Journal*, **2006**, 42, 740-750

18. Liang, D.; Hsiao, B.S.; Chu, B. *Adv Drug Delivery Rev.* **2007**, 59(14), 1392-1412

19. Grignard, Bruno; Vaillant, Alexandre; Coninck, Joel de; Piens, Marcel; Jonas, Alain M.; Jerome, Christine; Detrembleur, C. *Langmuir* **2011**, 27(1), 335-342

20. Ma, Minglin et al. *Langmuir* **2005**, 21, 5549-5554

21. Chiu, Yu-Cheng; Chen, Yougen; Kuo, Chi-Ching; Tung, Shih-Huang; Kakuchi, Toyoji; Chen, Wen-Chang *Appl. Mater. Interfaces* **2012**, 4, 3387-3395

22. Kim, Kwangsok; Yu, Meiki; Zong, Xinhua; Chiu, Jonathan; Fang, Dufei; Chu, Benjamin; Hadjiargyrou, Michael; Seo, Young-Soo; Hsiao, Benjamin S. *Biomaterials* **2003**, 24, 4977-4985

23. Wei, Ming; Kang, Bongwoo; Sung, Changmo; Mead, J. *Macromol. Mater. Eng*. **2006**, 291, 1307-1314

24. Detta, N.; El-Fattah, A.A.; Chiellini, E.; Walkenstrom, P.; Gatenholm, P. *Journal of Applied Polymer Science* **2008**, 110, 253-261

25. Nykanen, Antti; Hirvonen, Sami-Pekka; Tenhu, Heikki; Mezzenga, Raffaele; Ruokolainen, Janne; doi: 10.1002/pi.4559

26. Fong, Hao; Reneker, Darrell H. *Journal of Polymer Science: Part B: Polymer Physics* **1999**, 37, 3488-3493

27. Nguyen, Tuan-Anh; Jun, Tae-Sun; Rashid, Muhammad; Shin Kim, Y. *Material Letters* **2011**, 65, 2823-2825

28. Joo, W.; Kim, H.J.; Kim, J.K. *Langmuir* **2010**, 26(7), 5110-5114

29. Kasarova, S.K.; Sultanova, N.G.; Ivanov, C.D.; Nikolov, I.D. *Optical Materials* **2007**, 29, 1481–1490

30. Pillay, V. et. al. *Journal of Nanomaterials* **2013**

31. http://mee-inc.com/sem.html

32. Huttner, S.; Sommer, M.; Chiche, A.; Krausch, G.; Steiner, U.; Thelakkat, M. *Soft Matter* **2009**, 5, 4206-4211

33. http://en.wikipedia.org/wiki/Fourier_transform_infrared_spectroscopy

34. http://www2.ups.edu/faculty/hanson/Spectroscopy/IR/IRfrequencies.html

35. Rahman, M.A.; Amin, S.M.R.; Alam, A.M.S. *J. Sci.***2012,** 60(2), 185-189

36. Renugadevi, N.; Sangeetha, R.; Lalitha, P. *Arch. Appl. Sci. Res.* **2011***,* 3(3)*,* 492-498

37. Renugadevi, N.; Sangeetha, R.; Lalitha, P. *Adv. Appl. Sci. Res.* **2011**, 2(4), 629-641

38. Khan, T.A.; Singh, V.V.; Kumar, D. *J. Sci. Ind. Res.* **2004**, 63, 355-364